DRAG REDUCTION BY MEANS OF AN ARRAY OF STAGGERED CIRCULAR CAVITIES

Francesco Scarano
Dep. of Aerodynamics and Propulsion
ISAE - SUPAERO
10 Av. Belin, 31400 Toulouse France
francesco.scarano@isae-supaero.fr

Erwin R. Gowree
Dep. of Aerodynamics and Propulsion
ISAE - SUPAERO
10 Av. Belin, 31400 Toulouse France

Marc C. Jacob
Lab. de Mécanique des Fluides et
d'Acoustique, UMR 5509 CNRS, Université de
Lyon, Ecole Centrale de Lyon, INSA Lyon,
Université Claude Bernard Lyon I, 36 Av. Guy
de Collongue, 69130 Ecully, France

ABSTRACT

Further insight into the physics of boundary layer developing over perforated plates at moderate Reynolds numbers is gained from a combined experimental and numerical investigation. The findings are consistent with literature as to the possibility of reducing drag with circular perforations. Indeed, experimental results evidence a modification of the mean velocity profile, a reduction of the burst intensity and a thickening of the viscous sublayer. In contrast to other studies, the skin friction reduction is more pronounced when increasing the open area ratio, which is achieved by increasing the cavity diameter or equivalently by decreasing the inter-cavity spacing. The numerical investigations reveal spanwise patterns promoted by the perforations, which resemble those generated by spanwise wall oscillations and could explain the reduction in turbulent activity observed experimentally.

INTRODUCTION

The control of turbulent skin friction drag is a crucial task that can have a significant importance both in aeronautical context, where minimising the skin friction drag would have an impact on greenhouse gas emissions (Ricco *et al.*, 2021; Leschziner, 2020), as well as in the design of thermal insulators and heat exchangers.

Skin friction drag reduction mechanisms started to gain interest in the 80's, the majority of the techniques are based on the modification or disruption of the near wall turbulent cycle; this usually manifests in the attenuation of the turbulent activity (namely sweep ($u > 0$, $v < 0$) and ejections ($u < 0$, $v > 0$) altogether known as bursts) and the consequent reduction of the Reynolds shear stress.

Techniques such as riblets (García-Mayoral & Jiménez, 2011), and spanwise wall oscillation (Marusic *et al.*, 2021) have proven to be effective in reducing skin friction. The riblets hinder the spanwise movement of the coherent structures inside the boundary layer and have a charateristic size (spacing and height) which is between 10 and 20 viscous units (ν/U_τ, where U_τ is the friction velocity). The spanwise wall oscillations technique consists in imposing a spanwise modulation of the flow with a wavelength which is between 200 and 8000 wall units; the consequence is an attenuation of the turbulent activity thus a skin friction reduction. The practical implementation of the spanwise oscillations, in both real and laboratory conditions, is limited by the high complexity of the setup and the need of using an active forcing (Auteri *et al.*, 2010; Marusic *et al.*, 2021).

Skin friction drag reduction can be achieved either by reducing the Reynolds shear stress or by enhancing the wall-normal convection term (see the FIK equation (Fukagata *et al.*, 2002)). The enhancement of the wall-normal convection term explains the skin friction drag reduction in presence of wall-normal blowing (Kametani *et al.*, 2015) despite the increase in Reynolds shear stress.

Recent studies conducted on large dimples (van Nesselrooij *et al.*, 2016) (diameters up to four times the boundary layer thickness) and cavities (Bhat *et al.*, 2021; Silvestri *et al.*, 2017; Gowree *et al.*, 2019) (diameter in wall units $20 < d^+ < 145$) demonstrated the possibility of obtaining a significant drag or turbulent activity reduction at certain Reynolds numbers. The mechanism involved is not completely clear and it is sometimes associated with a passive jetting phenomenon (especially when the cavities are connected to a backing cavity) that dampens the wall normal velocity fluctuations reducing the Reynolds shear stress (Bhat *et al.*, 2021), or the property of an array of orifices to absorb turbulent activity (bursts) in a similar manner as they absorb acoustic fluctuations (Silvestri *et al.*, 2017). Another explanation (van Nesselrooij *et al.*, 2016) is that the cavities or dimples create what is sometimes called "meandering motion" that disrupts the near wall turbulent cycle.

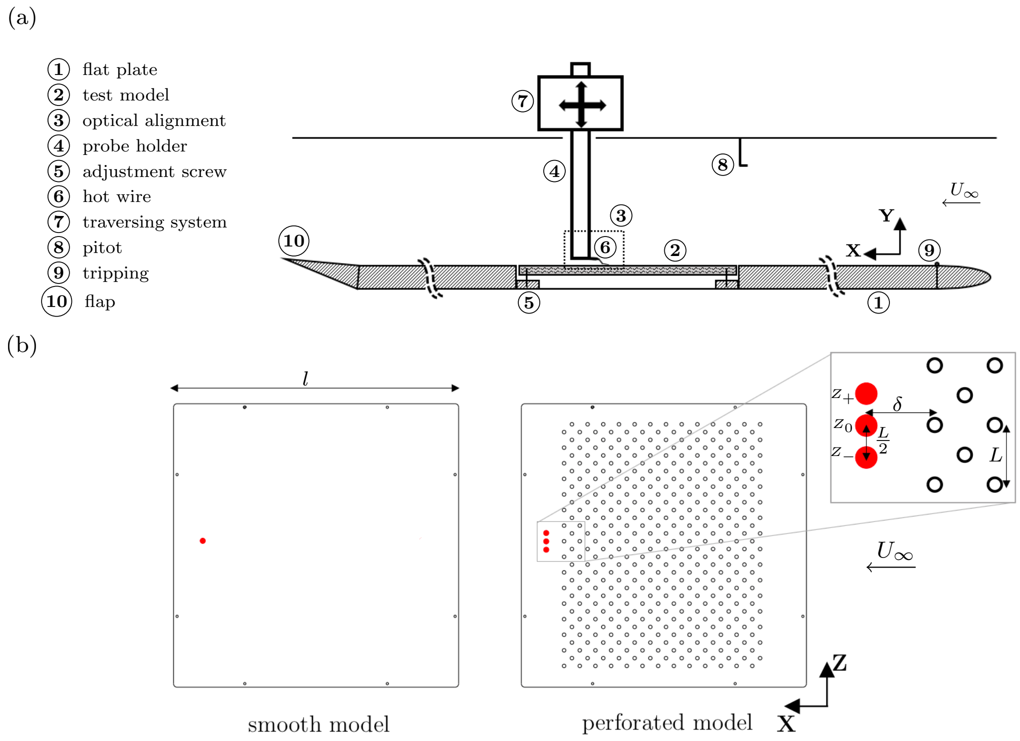

Figure 1. Experimental setup a) and test models b).

CASE	d^+			L^+			OAR
d3L11	85	115	150	305	425	540	0.1168
d4L11	110	155	200	305	425	540	0.2077
d5L11	140	190	245	305	425	540	0.3245
d6L11	165	230	295	305	425	540	0.4673
d3L07	85	115	150	195	270	345	0.2885
d3L11	85	115	150	305	425	540	0.1168
d3L16	85	115	150	445	615	790	0.0552
d3L22	85	115	150	610	850	1080	0.0292
d5L22	140	190	245	610	850	1080	0.0811

Table 1. Flow and geometrical parameters for the three different test conditions, downstream measurement location.

OBJECTIVES AND SETUP

With the aim to further prove the application of staggered cavities as a skin friction drag reduction technique, accurate boundary layer surveys are conducted in the low Reynolds number wind tunnel of ISAE-SUPAERO on a flat plate equipped with a square insert panel ($l = 400\,\mathrm{mm}$) which varies from a smooth baseline surface to models with arrays of circular cavities (Fig. 1). A zero pressure gradient is ensured by the deflection of a flap at the trailing edge of the flat plate (acceleration parameter smaller than 10^{-7}). Optical monitoring ensured precise measurements of the probe-to-wall distance (Gowree *et al.* (2015)). The perforated model is composed of a staggered array of cavities that have a fixed depth of 4 mm, a diameter between 3 and 6 mm, a stagger angle of 45° and a cavity spacing ranging between 7 and 22 mm. The measurements have been performed one boundary layer thickness (δ) downstream of the last row of cavities in the direct wake of a cavity (Z_0) and in the two spanwise locations (Z_+ and Z_-). Three flow conditions were tested 10, 15 and 20 m/s at which the Reynolds number based on the momentum thickness for the smooth case is respectively $Re_\theta = 1830, 2710$ and 3380. The values in wall units of the diameter d^+ and the cavity spacing L^+ calculated with the smooth friction velocity are reported in **Table 1** together with the open area ratio (OAR). They have been chosen in agreement with previous studies Gowree *et al.* (2019); Silvestri *et al.* (2017).

In order to better understand the three-dimensional mean flow topology, a large eddy simulation (LES) of a portion of the experimental domain is conducted with the code IC3 (Grébert *et al.*, 2017) using the experimental mean velocity profile as inlet condition. The lack of synthetic turbulence at the inlet limited this study to the mean flow quantities. The numerical domain keeps the same geometrical parameters but it is limited to three rows of cavities. The numerical simulation has been carried on one configuration only, the *d5L22* (5 mm diameter, 22 mm spacing).

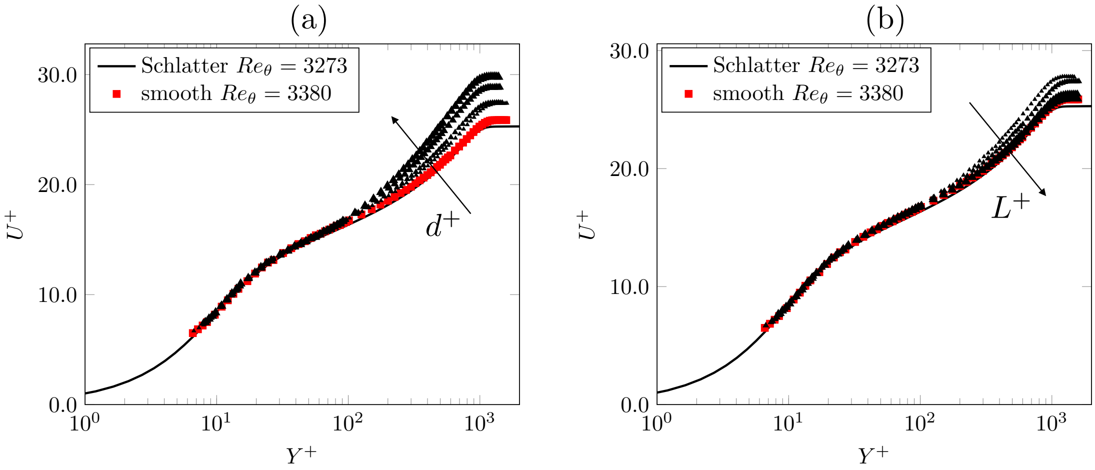

Figure 2. Mean streamwise velocity in wall units at the trailing edge of the model for the Z_0 location at 20 m/s, actual friction velocity is used, size of markers represents the increase in d^+/L^+, a) effect of d^+ for fixed L^+, b) effect of L_+ for fixed d^+, the in creasing values of d^+, and L^+ respectively are indicated by the arrows.

RESULTS AND DISCUSSION

The mean velocity profiles in wall units at the measurement location Z_0 are reported in Fig. 2 for a 20 m/s free stream velocity. The friction velocity U_τ is obtained with the Clauser chart technique by a fit of the mean profiles with the Spalding equation (Kendall & Koochesfahani, 2008) with $k = 1$ and $B = 5.5$. The actual friction velocity is used to non-dimensionalise in inner units all the statistics as well as all the geometrical parameters reported from now on. The profile in red represents the smooth baseline and shows a good match with the numerical results by Schlatter & Orlu (2010). The profiles for the perforated cases are plotted in black using different dimensions for the markers, bigger markers represents larger values of d^+ or L^+. The mean velocity profiles exhibit a mild deviation from the smooth baseline, which is more evident in the wake region. The effect is more pronounced for larger values of d^+ and for smaller values of L^+. For the largest values of L^+ (cavities furthest) the smooth condition is almost retrieved.

The friction coefficient C_f is computed from $C_f = 2\left(\frac{U_\tau}{U_\infty}\right)^2$. In Fig. 3 a) the variation of the local friction coefficient with respect to the smooth baseline case is plotted against the d^+. A local skin friction reduction is found for all the flow conditions; the skin friction reduction increases with d^+. An opposite trend is present when plotting the variation of skin friction coefficient against L^+ (not shown). In Fig. 3 b) the local skin friction reduction is plot against the OAR. The data show an overall decreasing trend which confirms that having a more dense array of cavities (increasing the OAR) has a beneficial effect on the skin friction drag. When increasing the OAR the boundary layer thickens and the momentum thickness increases with respect to the smooth case, Fig. 3 c). A similar trend is documented for the shape factor H, suggesting that the profiles are fuller. The plots against OAR appear more scattered with respect to the ones against d^+ or L^+, one reason could be that the OAR has been varied by changing two different parameters (diameter and spacing).

The Variable Interval Time Averaging (VITA) technique has been applied to the profiles (Blackwelder & Kaplan, 1976). This technique allows to detect shear events in a turbulent boundary layer which can be associated to bursts. The short-term RMS is compared to the long-term RMS of the entire signal. If the short-term RMS is larger than the long-term RMS multiplied by a constant k a burst is detected (Sullivan & Pollard (1996)). The short-term RMS is computed considering a time window which has to be of the order of magnitude of the characteristic time of the passage of a structure ($T^+ \cong 20$), where $T^+ = \frac{Tu_\tau^2}{\nu}$. Given a fluctuating quantity $Q(x_i,t)$ the short term average of the variable in the interval time T can be defined as

$$\widehat{Q}(x_i,t,T) = \int_{t-\frac{T}{2}}^{t+\frac{T}{2}} Q(x_i,s)ds \qquad (1)$$

and the short term variance is

$$\widehat{\mathrm{var}}(x_i,t,T) = \widehat{U^2}(x_i,t,T) - [\widehat{U}(x_i,t,T)]^2. \qquad (2)$$

The detection is then based on a Heaviside function

$$D(t) = 1 \quad \text{if} \quad \widehat{\mathrm{var}}(x_i,t,T) > k \cdot \sigma_u^2; \quad 0 \quad \text{otherwise} \qquad (3)$$

where σ_u^2 is the variance of the entire signal. For each value of Y^+ it is possible to obtain the conditional streamwise velocity namely the average burst. The burst intensity can be defined as the peak-to-peak value of the conditional streamwise velocity (Silvestri *et al.*, 2017). In Fig. 4 the intensity profiles are reported for 10 m/s when varying a) the d^+, b) L^+. As for the mean velocity profiles, the effect is more pronounced for large values of d^+ and small values of L^+ which correspond to higher OAR. For the small d^+ as well as large L^+ the smooth intensity profile is almost retrieved.

The root mean square of the streamwise velocity in wall units σ_u^+ is reported in Fig. 7 for the case *d5L11* at 10 m/s and compared with the smooth baseline case. The inner peak appears unchanged both in position and in magnitude when the actual friction velocity is employed, although not shown here, the peak is lower with respect to the smooth case when the friction velocity of the smooth case is used. The presence of a second peak around $Y^+ = 100$, again this behaviour is more pronounced when increasing the d^+ (not shown here).

Similar considerations can be made when looking at the two dimensional (2D) premultiplied power-spectra, shown in

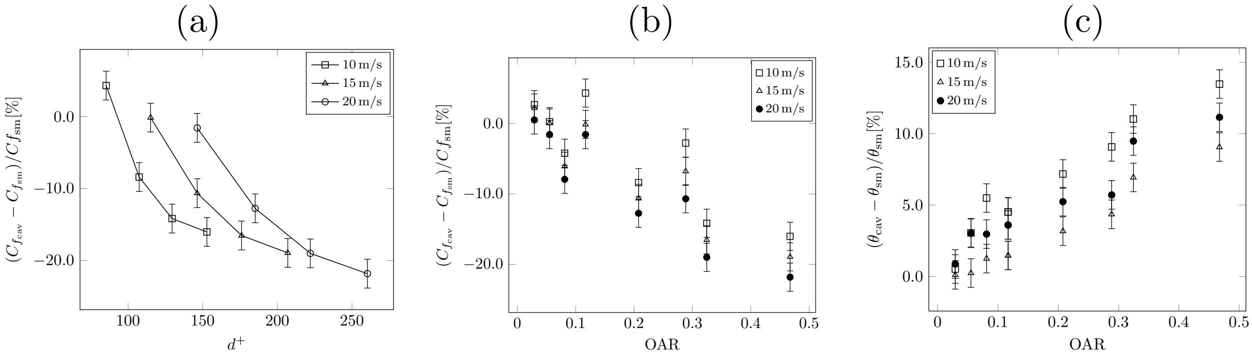

Figure 3. Skin friction coefficient percentage variation, a) effect of d^+ at the three flow conditions, b) effect of the OAR, c) momentum thickness percentage variation between perforated and smooth, effect of OAR.

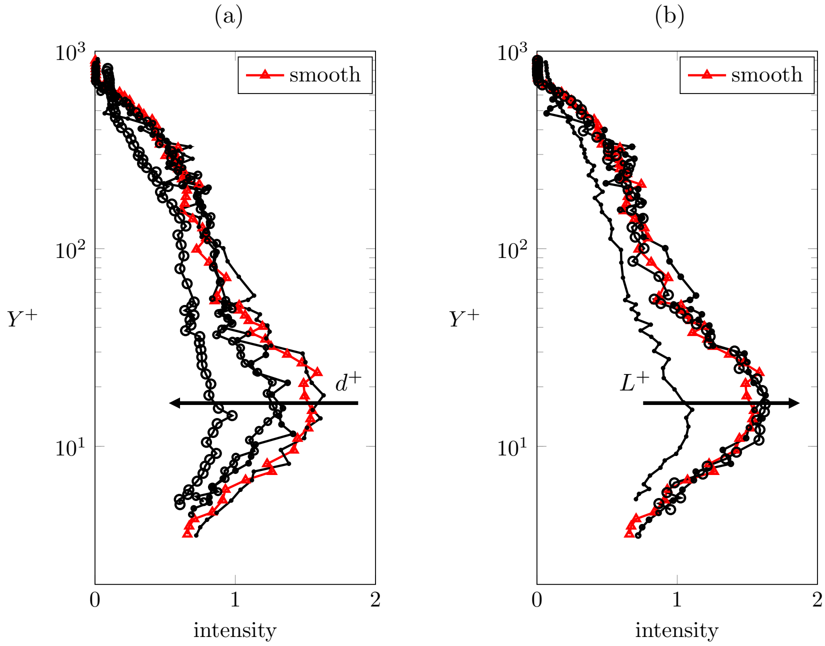

Figure 4. VITA intensity profile at 10 m/s, increasing size of the circles (and following the arrows) represents the increase in d^+ and L^+, a) effect of d^+, b) effect of L^+.

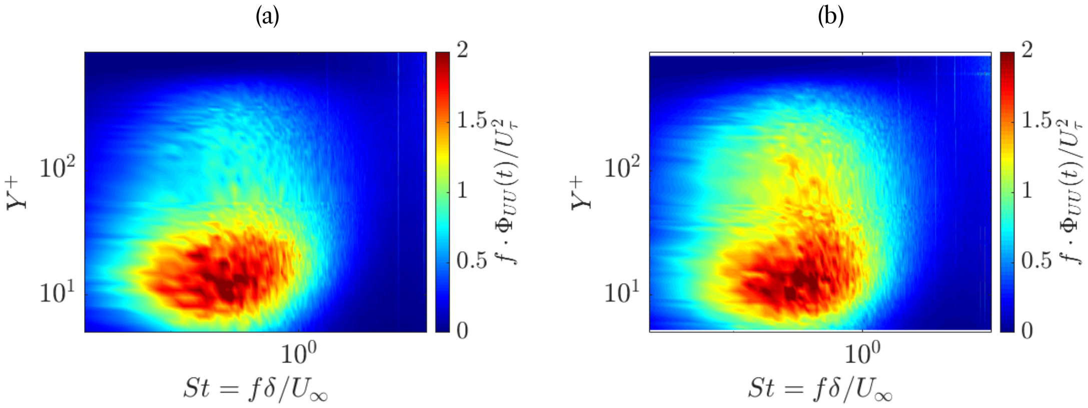

Figure 5. 2D premultiplied turbulence spectra of the streamwise velocity fluctuation non-dimensionalised by the actual friction velocity at 10 m/s a) smooth baseline, b) *d5L11* case.

Fig. 5. The energy distribution is affected by the cavities with the presence of a second peak around $Y^+ = 100$. This suggests that the cavities act to increase the energy of the outer-layer structures.

The effect of the measurement locations Z_+ and Z_- with respect to Z_0 is addressed in Fig. 6 only for the case *d6L11* (where the most significant skin friction variation is found) but similar considerations can be made for all the cases tested.

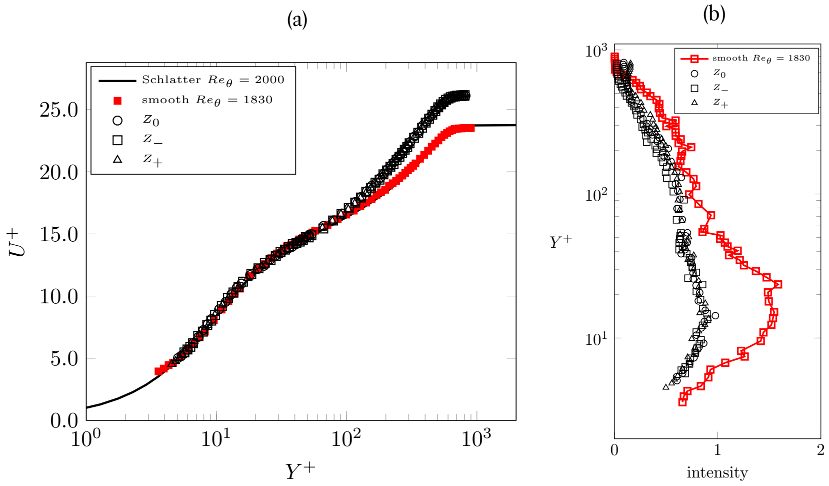

Figure 6. Effect of spanwise measurement location on a) mean streamwise velocity profile, b) VITA intensity profile.

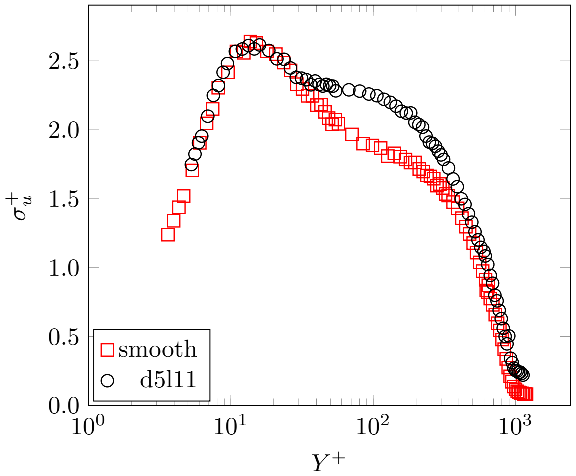

Figure 7. Root mean square of the streamwise velocity in wall units at the trailing edge of the model at 10 m/s, comparison between smooth baseline and *d5L11*, actual friction velocity is used.

Both in the mean velocity profiles and the intensity profiles the three measurements (Z_0, Z_+, Z_-) are indistinguishable. This result confirms that the skin friction reduction is not just a local artefact but that it is uniform along the span.

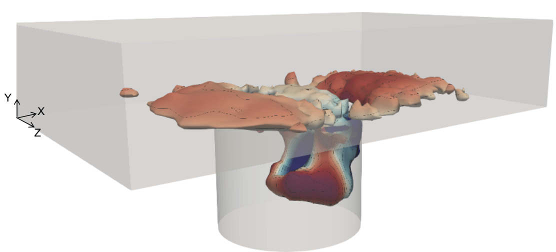

Figure 8. Iso-surface of the Q-criterion *d5L22* at 10 m/s, coloured by the contour of $V/U_\infty \times 100$ from -5% (blue) to 5% (red).

The numerical results, limited to the case *d5L22*, reveal the generation of a counter-rotating vortex pair and a recirculating flow inside each cavity, as shown in Fig. 8. These structures bend the streamlines in the vicinity of the perforations thus generating a steady streamwise and spanwise velocity pattern in the near wall region (Fig. 9.a).

The streamwise evolution along the yellow dotted line of the spanwise mean velocity is plotted in Fig. 9.b: it shows a remarkable similarity with the evolution resulting from a near wall spanwise forcing as reported by Marusic *et al.* (2021). According to these authors, drag reduction can be obtained by imposing an upstream travelling wave at the wall:

$$W(x,t) = A\cos\left(\frac{2\pi}{\lambda_x}x - \frac{2\pi}{T}t\right) \quad (4)$$

where A is the amplitude of the oscillation, λ_x is the wavelength and T is the period of the oscillation. A steady version of the technique, introduced by Viotti *et al.* (2009), has proven to be effective and leads to a drag reduction (up to 52%) by generating a spatial Stokes layer that disrupts the near wall turbulent cycle.

The main differences with respect to the results reported by Viotti *et al.* (2009) are the smaller amplitude of the oscillations and the different spanwise profiles (Fig. 9.c), coupled with the fact that here the flow is at rest at the wall due to the no-slip condition, but it was not zero in the case of Viotti *et al.* (2009) due to the oscillating wall condition. The current numerical results show that the wavelength λ_x^+ is imposed by the streamwise spacing of the cavities and that it lies in the range of the wavelengths for which drag reduction is reported by Viotti *et al.* ($200 < \lambda_x^+ < 8000$).

The results however evidence several similarities with uniform blowing (Kametani *et al.*, 2015): the shape of the mean velocity profile, the increase of the thickness and the shape factor. In addition, the presence of a second peak in the premultiplied power spectrum at $Y^+ = 100$ and the increase in the root mean square of the freestream velocity for the same location suggest an increase in the energy content of the outer structures. The mechanism for skin friction reduction by means of blowing is completely different with respect to the spanwise wall oscillations. In fact, as mentioned in the introduction, the skin friction reduction is achieved by the reduction of the mean wall-normal convection term which overcomes the

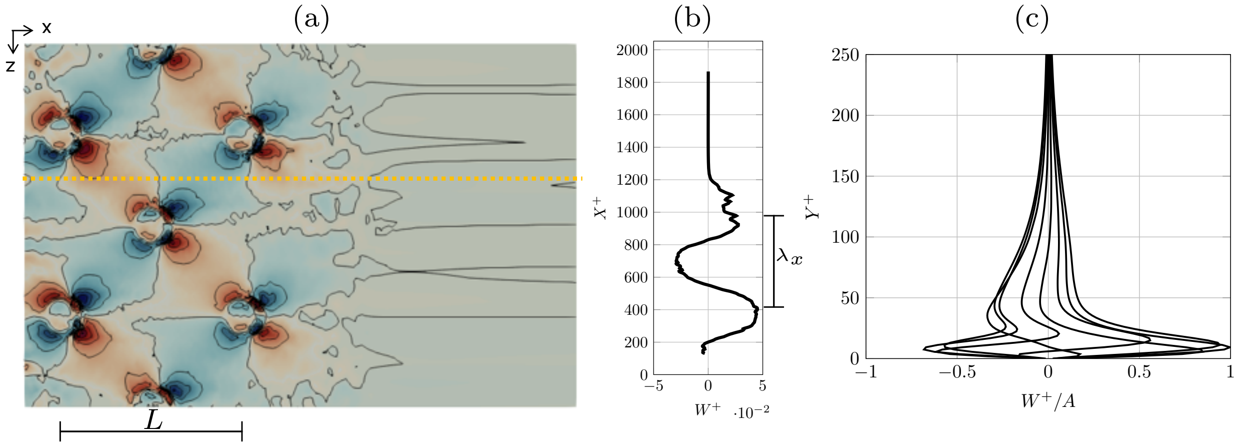

Figure 9. Spanwise mean flow from the numerical simulation at 10 m/s for *d5L22*, slice at $y^+ = 5$ parallel to the wall, contour of W/U_{inf} between -1.5 and 1.5 % a), spanwise flow evolution along the dashed line b), spanwise profiles at discrete streamwise locations c).

increase of the turbulent (Reynolds shear stress) term. The suction acts in the opposite way, it dampens the Reynolds shear stress contribution but increases the mean wall-normal convection leading to a skin friction increase (Kametani *et al.*, 2015). However, despite the similarities in the results, it is rather difficult to link the topology inside the cavity with uniform blowing. The recirculation inside the cavity, in fact, does not affect the total wall-normal mass flow rate. For this reason if the cavities create a blowing they should create an equal amount of suction, if this is the case therefore it is unlikely that the reduction due to the blowing will overcome the increase due to the suction.

A possible explanation is that the blowing phenomenon is not created by the recirculating vortex but by some sort of resonance which acts in certain conditions (particular diameter-to-height ratio or a certain value of the impinging boundary layer). This could potentially generate an unsteady and non-uniform blowing. Similar results have been recently documented by Bhat *et al.* (2021) for small cavities backed by another cavity. Despite the mean velocity flux through all holes being negligible, instantaneous upward and downward components through the holes are reported. The direction of the flow is influenced by the structures immediately above the cavities, resulting in a dampening of the Reynolds shear stress and a consequent skin friction reduction.

What has to be underlined is the difference between the current results and the findings of Silvestri *et al.* (2017) and Gowree *et al.* (2019). In the work of Silvestri *et al.* (2017) the cavities are not staggered, they are designed to match the dimensions of the coherent structures in a boundary layer (the spacing is 100 viscous units in the spanwise direction and 1000 in the streamwise direction). A decrease of burst intensity is documented up to a certain value of the cavity diameter in wall units ($d^+ = 145$). The explanation given by the authors is that the cavities ingest the sweeps thus reducing the skin friction. If the cavities are too big the shear layer above the cavities breaks , which reduces drag benefit. Gowree *et al.* (2019) evidenced a pefrormance loss when increasing the Reynolds number based on the cavity diameter. In the current study changing the Reynolds number (obtained by changing the velocity) has only a weak effect on the performances. What has to be underlined are the completely different trends with respect to the study of Silvestri *et al.* (2017). The current results evidence an increase of the performance when d^+ is increased and L^+ is decreased. The overall behaviour appears to be governed by the concentration of cavities namely by the OAR parameter. In the current investigation, the drag reduction benefit persisted for all the conditions tested.

SUMMARY

The current results confirm the possibility of using a staggered array of cavities as a skin friction reduction technique. A modification of the mean velocity profiles and an intensity reduction of the burst is evidenced. The skin friction reduction is more pronounced when increasing the d^+ and when decreasing L^+, namely when the Open Area Ratio is increased. Another effect of the cavities is to thicken the boundary layer and to increase the shape factor. This effect is more pronounced for larger OAR. The premultiplied spectra evidence an effect of the cavities in the outer layer with the presence of a second peak around $Y^+ = 100$. The current results shows similarities with uniform blowing however this link cannot be fully supported by the flow topology. However, the 3D flow topology arising from the numerical simulation shows that the cavities are equivalent to a generator of steady spanwise flow oscillations in the streamwise direction. The measurements at different spanwise locations (Z_0, Z_+, Z_-) provide some confidence that the skin friction reduction is not just a local artefact in the wake of the cavities but can be considered uniform along the span.

REFERENCES

Auteri, F., Baron, A., Belan, M., Campanardi, G. & Quadrio, M. 2010 Experimental assessment of drag reduction by traveling waves in a turbulent pipe flow. *Physics of Fluids* **22** (11), 115103.

Bhat, S. S., Silvestri, A., Cazzolato, B. S. & Arjomandi, M. 2021 Mechanism of control of the near-wall turbulence using a micro-cavity array. *Physics of Fluids* **33** (7), 075114.

Blackwelder, R. F. & Kaplan, R. E. 1976 On the wall structure of the turbulent boundary layer. *Journal of Fluid Mechanics* **76** (1), 89–112.

Fukagata, Koji, Iwamoto, Kaoru & Kasagi, Nobuhide 2002 Contribution of reynolds stress distribution to the skin friction in wall-bounded flows. *Physics of Fluids* **14** (11), L73–L76.

García-Mayoral, Ricardo & Jiménez, Javier 2011 Drag reduction by riblets. *Philosophical Transactions of the Royal Society A: Mathematical, Physical and Engineering Sciences* **369** (1940), 1412–1427.

Gowree, Erwin, Atkin, Chris & Gruppetta, S 2015 A simple digital-optical system to improve accuracy of hot-wire measurements. *Measurement Science and Technology* **26**.

Gowree, E.R., Jagadeesh, C. & Atkin, C.J. 2019 Skin friction drag reduction over staggered three dimensional cavities. *Aerospace Science and Technology* **84**, 520–529.

Grébert, A., Bodart, J., Jamme, S. & Joly, L. 2017 Simulations of shock wave/turbulent boundary layer interaction with upstream micro vortex generators. In *10th International Symposium on Turbulence and Shear Flow Phenomena*.

Kametani, Yukinori, Fukagata, Koji, Örlü, Ramis & Schlatter, Philipp 2015 Effect of uniform blowing/suction in a turbulent boundary layer at moderate reynolds number. *International Journal of Heat and Fluid Flow* **55**, 132–142.

Kendall, Anthony & Koochesfahani, Manoochehr 2008 A method for estimating wall friction in turbulent wall-bounded flows. *Experiments in Fluids* **44**, 773–780.

Leschziner, Michael A. 2020 Friction-drag reduction by transverse wall motion – a review. *Journal of Mechanics* **36** (5), 649–663.

Marusic, Ivan, Chandran, Dileep, Rouhi, Amirreza, fu, Matt, Wine, David, Holloway, Brian, Chung, Daniel & Smits, Alexander 2021 An energy-efficient pathway to turbulent drag reduction. *Nature Communications* **12**.

van Nesselrooij, M., Veldhuis, L. L. M., van Oudheusden, B. W. & Schrijer, F. F. J. 2016 Drag reduction by means of dimpled surfaces in turbulent boundary layers. *Experiments in Fluids* **57** (9), 142.

Ricco, Pierre, Skote, Martin & Leschziner, Michael A 2021 A review of turbulent skin-friction drag reduction by near-wall transverse forcing. *arXiv preprint arXiv:2103.04719* .

Schlatter, P. & Orlu, R. 2010 Assessment of direct numerical simulation data of turbulent boundary layers. *Journal of Fluid Mechanics* **659**, 116–126.

Silvestri, Anton, Ghanadi, Farzin, Arjomandi, Maziar, Cazzolato, Ben & Zander, Anthony 2017 Attenuation of sweep events in a turbulent boundary layer using micro-cavities. *Experiments in Fluids* **58**.

Sullivan, P & Pollard, A 1996 Coherent structure identification from the analysis of hot-wire data. *Measurement Science and Technology* **7** (10), 1498–1516.

Viotti, Claudio, Quadrio, Maurizio & Luchini, Paolo 2009 Streamwise oscillation of spanwise velocity at the wall of a channel for turbulent drag reduction. *Physics of Fluids* **21** (11), 115109.